Role of Gd^{3+} concentration on the structure, transport and magnetic properties of (Ni-Ti) doped Mn-Zn nanocystalline ferrite

K. E. Rady

Engineering Basic Sciences Department, Faculty of Engineering, Menoufia University, Shebin El- Kom, Egypt.

Abstract: A system of general chemical formula $Mn_{0.9}Zn_{0.1}(Ni\text{-}Ti)_{0.05}Gd_yFe_{1.9-y}O_4$; $(0.0 \leq y \leq 0.05)$ were prepared using standard ceramic method. The structure of the prepared samples was indicated using XRD diffraction. The average crystallite size of the prepared samples was estimated using Scherrer's equation and ranged from 96 to 104nm. DC electrical resistivity of the prepared samples was measured at room temperature using the two probe method. The thermoelectric power measurements show n-type conduction for all the prepared samples. The substitution of Fe^{3+} ions by Gd^{3+} ions improves the physical properties by increasing resistivity and consequently decreasing the dielectric loss so, they can be used in the core transformers. Also, the effect of temperature on the initial magnetic permeability was studied. Finally the cation distribution of the prepared samples was assumed and the theoretical magnetic moment was also calculated and compared with the experimental one. The substitution by Gd^{3+} improves the physical properties of the prepared samples where the sample of y= 0.01 exhibits high resistivity, highest initial permeability.

Keywords: Rare earth ferrites; SEM; magnetic moment; magnetic permeability; electrical resistivity; cation distribution; thermoelectric power; magnetic moment

1. Introduction

Physical properties of ferrites are very important not only from the application point of view but also from the fundamental point of view. Study of the magnetic and dielectric properties of ferrites and analysis of results may help in producing composites for various applications. Mixed ferrites such as Mn-Zn ferrites are attractive materials for microwave device applications due to their large magnetic permeability in the radio frequency region high Curie temperature, high mechanical hardness, chemical stability at relatively low frequencies and low price, Hence, they are more important commercially.

Rare earth ferrites have found important applications in modern telecommunication and electronic devices. For this reason, engineers and scientists are interested in the study of rare earth ferrites to determine their characterization [1]. But these materials have low resistivity, and high eddy current loss due to the rapidly fluctuating magnetic field. So the influence of small additives on the crystal structures and the physical properties of some ferrite were studied by many authors [2-6].

Studies of Rezescu et al. [7] indicate that the integration of rare earth cations into the spinel structure of ferrite results in modification of electrical and magnetic properties. They investigate a lowering of the Curie temperature and saturation magnetization due to the substitution of iron with lanthanides, formation of a plateau in the temperature-dependent initial permeability curve and an increase in the specific dc resistivity. Additionally, micro-structural parameters like grain size and porosity were affected. The change in the magnetic properties compared to samples without rare earth has been interpreted in terms of microstructure parameters. In general, rare earth with large ionic radius ions cannot occupy the tetra- and octahedral sites [8]; during the sintering, these will form secondary phases on the grain boundaries. However, it should be emphasized that the process of dissolution of R_2O_3 in the spinel lattice may also

occur. So, the possibility of formation of compounds with inverse spinel structure, when R^{3+} substitutes Fe^{3+} on the octahedral sites [9].

The present work study the effect of Gd^{3+} ion substitution on the microstructure, transport and magnetic properties of $Mn_{0.9}Zn_{0.1}(Ni\text{-}Ti)_{0.05}Gd_yFe_{1.9-y}O_4$; $(0.0 \leq y \leq 0.05)$ to get the desired concentration of Gd^{3+} ions to obtain high physical properties to be used in the technological applications.

2. Experimental techniques

Ferrite with a general formula $Mn_{0.9}Zn_{0.1}(Ni\text{-}Ti)_{0.05}Gd_yFe_{1.9-y}O_4$; $(0.0 \leq y \leq 0.05$; step 0.01) was prepared by the standard ceramic technique. The structure of the prepared samples was identified using XRD on a Brucker axis D8 diffractometer of Cu-K_α radiation (λ =1.5418 Å). The equipment used for IR analysis is 1650 Perkin-Elmer to detect the IR absorption spectra for the samples with different concentrations. The two surfaces of each pellet were coated with silver paste and checked for good electrical contact. The dc resistivity of the prepared samples was measured at room temperature using the two-probe method as a function of temperature. The saturation magnetization of the prepared sample was measured using the vibrating sample magnetometer (VSM) of a magnetizing field ranging from 0 to 5000 Oe.

3. Results and discussion

3.1. Microstructure properties

3.1.1. X-ray diffraction

The Microstructure of the samples of general formula $Mn_{0.9}Zn_{0.1}(Ni\text{-}Ti)_{0.05}Gd_yFe_{1.9-y}O_4$ was indicated using XRD patterns as shown in **Fig. 1**. For $0.0 \leq y \leq 0.01$, the samples reveal a single phase cubic spinel structure while for $0.02 \leq y \leq 0.05$, a small amount of secondary phase clear with reflections formed besides with the main diffraction peaks. This peak of secondary phase was matched with those of $Gd_3Fe_5O_{12}$ according the ICDD card No: 48-0077[10]. The crystallographic planes of the main characteristic peaks of cubic spinel structure were perfectly matched with the theoretical data of Franklinite spinel structure (ICDD card No. 74-2402).

The average crystallite size of the prepared samples was estimated using Scherrer's equation [11] and ranged from 96 to 104 nm. The density (D) was calculated and shown in Fig (2).The density (D). It can be seen from figure that the density increases with increasing Gd content (y), the difference in atomic weight between Gd^{3+} ions (157.25amu) and Fe^{3+} ions (55.845amu) contributes to this increase in (D).

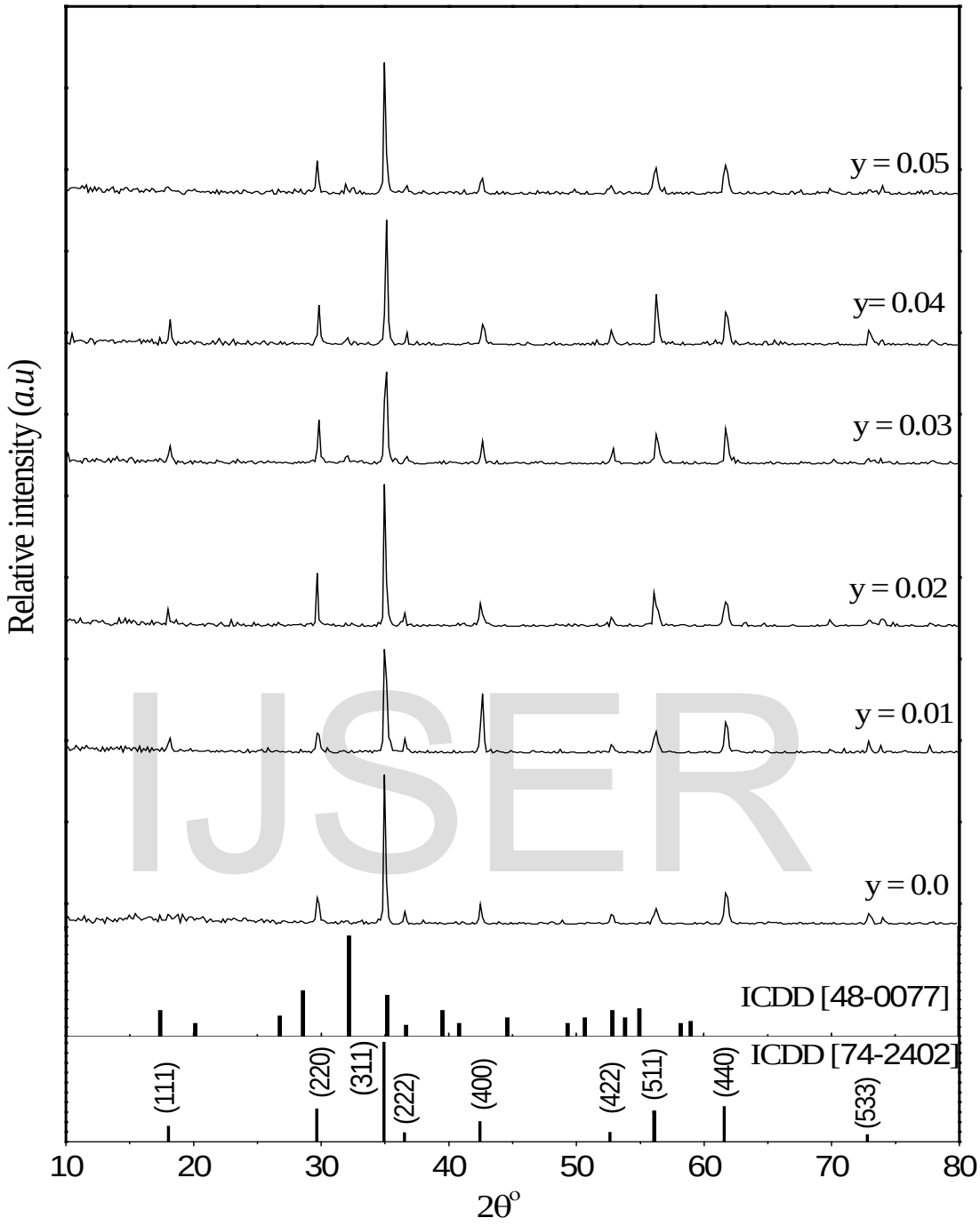

Fig.1. X-ray diffraction patterns of the prepared samples $Mn_{0.9}Zn_{0.1}(Ni\text{-}Ti)_{0.05}Gd_yFe_{1.9\text{-}y}O_4$

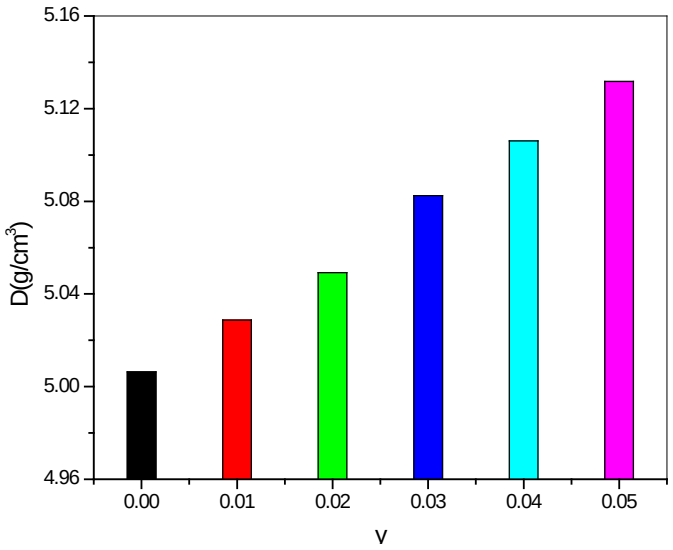

Fig. 2. Variation of the density of the prepared samples as a function of Gd content (y).

3.1.2. Infra-red spectra (IR)

Figure (3) shows that the IR spectra for $Mn_{0.9}Zn_{0.1}(Ni\text{-}Ti)_{0.05}Gd_yFe_{1.9-y}O_4$ ($0.0 \leq y \leq 0.05$) ferrites. The IR spectra are recorded in the range from 200-1000 cm^{-1}. The higher frequency band υ_1 (591-594 cm^{-1}) and lower frequency band υ_2 (383-394 cm^{-1}) corresponding to vibration of tetrahedral and octahedral complexes respectively [12]. These bands are mainly dependent on Fe-O distances and the nature of the cations involved. It is observed that with the increase of substitution of Gd^{3+} ions, the band frequency υ_2 is slightly shifted whereas negligible effect on υ_1 is found as observed in Table (1). This shift in υ_2 may be attributed to the Gd^{3+} ions substitution for Fe^{3+} ions on octahedral sites due to its higher atomic weight and larger ionic radius than Fe^{3+} ions which decreases the Fe^{3+} - O^{2-} distance on B sites [13]. When Gd^{3+} concentration $y \geq 0.02$, an extra phase probably ($Gd_3Fe_5O_{12}$) was observed and extra peaks in IR (971-982 cm^{-1}) were appeared [14], this confirms the extra peaks observed in XRD.

Table (1): Values of the transmission bands for the prepared samples $Mn_{0.9}Zn_{0.1}(Ni\text{-}Ti)_{0.05}Gd_yFe_{1.9-y}O_4$

Gd-content (y)	υ' cm^{-1}	υ_1 cm^{-1}	υ_2 cm^{-1}
0.0	---	591	394
0.01	---	592	392
0.02	---	594	390
0.03	982	594	387
0.04	971	593	385
0.05	976	594	383

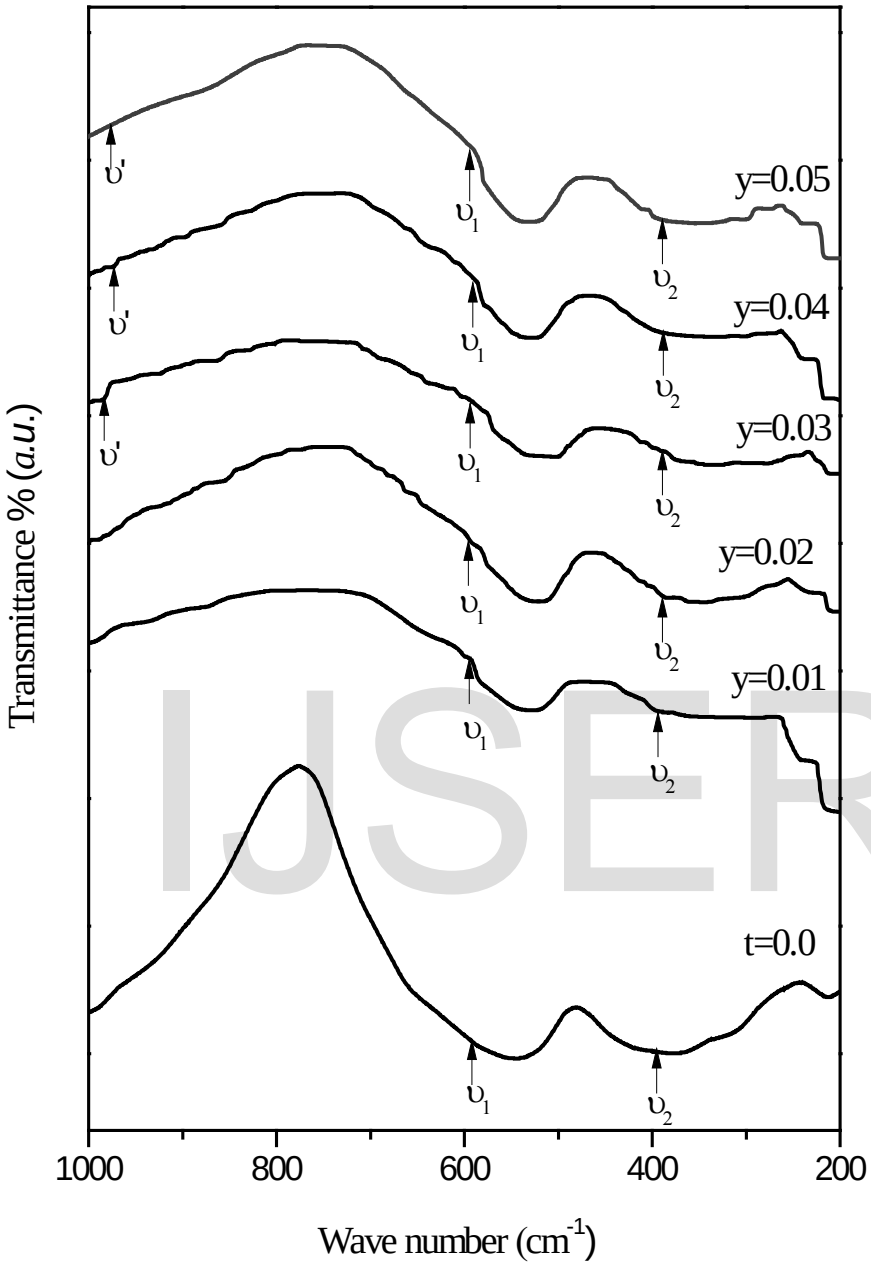

Fig. 3. IR transmission spectra of the prepared samples $Mn_{0.9}Zn_{0.1}(Ni\text{-}Ti)_{0.05}Gd_yFe_{1.9\text{-}y}O_4$

3.2. Transport properties

3.2.1. DC electrical resistivity

The DC electrical resistivity of the spinel system $Mn_{0.9}Zn_{0.1}(Ni\text{-}Ti)_{0.05}Gd_yFe_{1.9\text{-}y}O_4$ was measured at room temperature as a function of composition. Figure 4, shows that, the electrical resistivity (ρ) was found increasing gradually with the increasing of Gd content (y) from 8.8 $x10^3$ Ω.m to 19.2$x10^3$ Ω.m. The increasing of the resistivity with Gd^{3+} ions concentration can be explained according to that the Gd^{3+} ions reside on B-site hence Gd^{3+} ions will impede the electron exchange between Fe^{2+} and Fe^{3+} ions on B-sites. In addition, for higher Gd^{3+} ions substitution i.e. at $0.03 \leq y \leq 0.05$, the resistivity (ρ) also increases, this can be attributed to the Gd^{3+} ions enter partially into the lattice sites and the rest may reside at the grain boundary creating a secondary phase ($Gd_3Fe_5O_{12}$) as a large number of insulating grains boundaries surrounded spinel ferrite which oppose the electron flow [15]. The increase of the electrical resistivity for the investigated system reduces the occurrence of the eddy currents and consequently reduces the energy loss as a heat so they can be used in many applications such as transformer cores and memory cores. Similar results were obtained for Co-Ferrite [16].

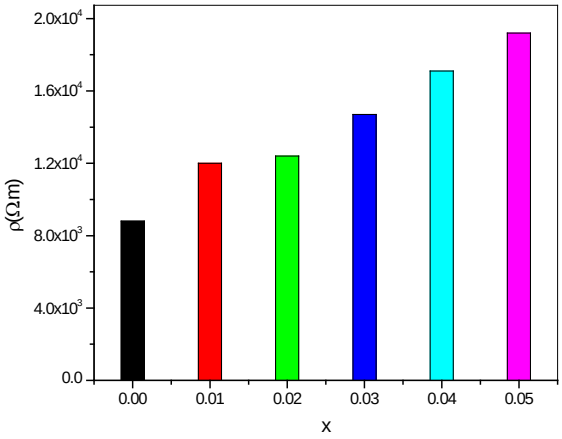

Fig. 4. Compositional dependence of the DC Electrical resistivity of the prepared samples

3.2.2. Seebeck voltage coefficient

The Seebeck voltage coefficient of the spinel system $Mn_{0.9}Zn_{0.1}(Ni\text{-}Ti)_{0.05}Gd_yFe_{1.9\text{-}y}O_4$ was studied as a function of absolute temperature, all the samples exhibits negative value of seebeck voltage coefficient as illustrated in **Fig. 5**. The hopping process between the metal ions of different valences is mainly due to electrons as indicates the semiconducting n-type behavior of all the investigated samples which is predominantly due to hopping of electron from Fe^{2+} to Fe^{3+} ions ($Fe^{2+} \leftrightarrow Fe^{3+} + e^-$) [17]. Introducing Gd^{3+} ions will affect the hopping process directly and the Gd^{3+} ions doped sample gives negative Seebeck coefficient due to small negative polarons that participate in the conduction process.

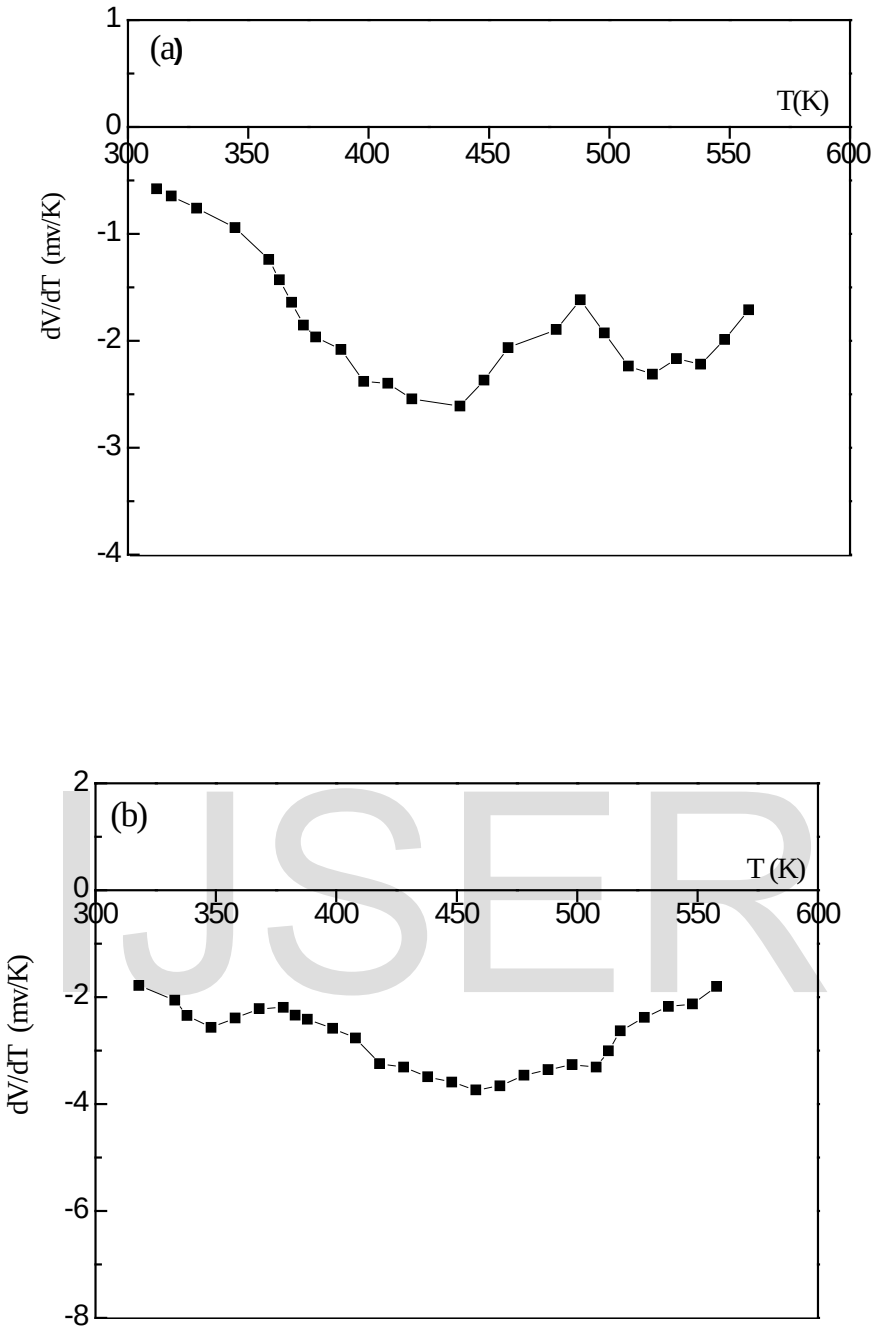

Fig.5. Seebeck voltage coefficient as a function of the average temperature of $Mn_{0.9}Zn_{0.1}(Ni\text{-}Ti)_{0.05}Gd_yFe_{1.9\text{-}y}O_4$, for a) y = 0.01, b) y = 0.04

3.3. Magnetic moment and initial magnetic permeability

The effect of temperature on the initial permeability (μ_i) of the prepared samples is shown in **Fig. 6**. This figure shows a sudden drop in the initial magnetic permeability at the Curie temperature T_C. The sharp drop in the initial permeability at Curie temperature reflects the good homogeneity of the prepared sample and is attributed to the magnetic transition from the ferromagnetic to paramagnetic state. This figure shows Also that all the curves are typical multi-domain grains. The compositional dependence of the initial permeability is shown in **Fig. 7**. This figure shows as Gd content increases the initial permeability increase up to y= 0.01 due to the high magnetic moment of Gd^{3+} compared with that of Fe^{3+}. For $y \geq 0.02$ as Gd content increases the initial permeability decreases then decreases. This behavior can be explained using the following approximate equation for the initial permeability [18]:

$$\mu_i = \frac{M_S^2 D}{\sqrt{K_1}} \qquad (1)$$

where D is the average grain diameter, M_s is the saturation magnetization and K_1 is the magneto-crystalline anisotropy constant. According to this equation, the decrease of the initial permeability is attributed to the decreases of the saturation magnetization due to the appearance of secondary phases at the grain boundaries.

The theoretical and experimental magnetic moment of the prepared samples were investigated and compared with each other. In order to calculate the theoretical magnetization of the prepared samples a cation distribution for the given system must be assumed. In general, Zn^{2+} ions have a higher preference for A-site, Ti^{4+}, Ni^{2+} and Gd^{3+} ions have higher preference for B-site while Fe^{3+} and Mn^{2+} ions are distributed between the tetrahedral and octahedral sites.[19] The assumed cation distribution can be written as:

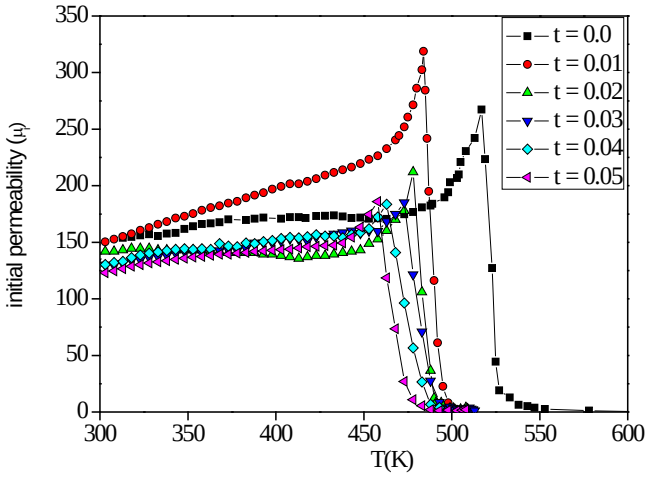

Fig.6. Variation of the initial permeability (μ_i) with absolute temperature T of $Mn_{0.9}Zn_{0.1}(Ni\text{-}Ti)Gd_yFe_{1.9-y}O_4$ system.

$$(Zn_{0.1}^{2+}Mn_{0.7}^{2+}Fe_{0.2}^{3+})[Mn_{0.2}^{2+}\,Ni_{0.05}^{2+}Ti_{0.05}^{4+}Gd_y^{3+}Fe_{1.7-y}^{3+}]\,O_4^{2-}$$

where the brackets ( ) and [ ] denote to A- and B- sites respectively.

According to Néel`s two sublattice model of ferrimagnetism, the magnetic moment n_B is expressed as [20]:

$$n_B = M_B - M_A$$

where M_B and M_A are B and A sublattice magnetic moment, respectively. Using the assumed cation distribution, the magnetic moments of A and B sites can be calculated using the following equations:

$M_A = 0.1M_{Zn}^{2+} + 0.7M_{Mn}^{2+} + 0.2M_{Fe}^{3+}$ (2)

$M_B = 0.2\,M_{Mn}^{2+} + 0.05\,M_{Ni}^{2+} + 0.05\,M_{Ti}^{4+} + (y)\,M_{Gd}^{3+} + (1.7\text{-}y)\,M_{Fe}^{3+}$ (3)

then, $n_B = 6.012 - 585y$

The experimental magnetic moment was calculated by means of the following relation [21]:

$$n_B = \frac{M M_s}{5585} \qquad (4)$$

where M is the molecular weight, Ms is the saturation magnetization measured using vibrating sample magnetometer. Figure 8 shows the change in theoretical and experimental magnetic moment in Bohr magnetron (BM) with Gd content. This figure shows that, as Gd-content increases the magnetic moment decreases. This behavior can be explained on the basis of the high magnetic moment of the Gd^{3+} ions is effective only at very low temperature but the Gd^{3+} ions seems as non-magnetic ions at room temperature [22,23]. So, the replacement of Fe^{3+} ions by Gd^{3+} ions in the octahedral sites produces a decrease in the magnetic moment of the octahedral site (M_B) and consequently the total magnetic moment ($n_B = M_B - M_A$) decreases. Figure 8 shows also that, the experimental magnetic moment is greater than theoretical one, which can be attributed to the formation of Fe^{2+} ions of smaller magnetic moment during the sintering process.

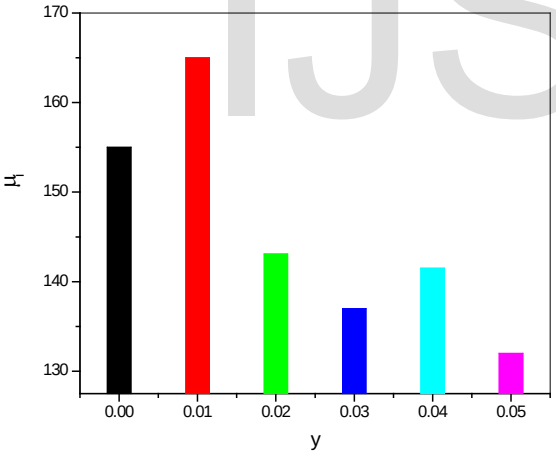

Fig. 7. Variation of the initial permeability (μ_i) with Gd content (y) of $Mn_{0.9}Zn_{0.1}(Ni\text{-}Ti)_{0.05}\ Gd_yFe_{1.9-y}O_4$ system at room temperature.

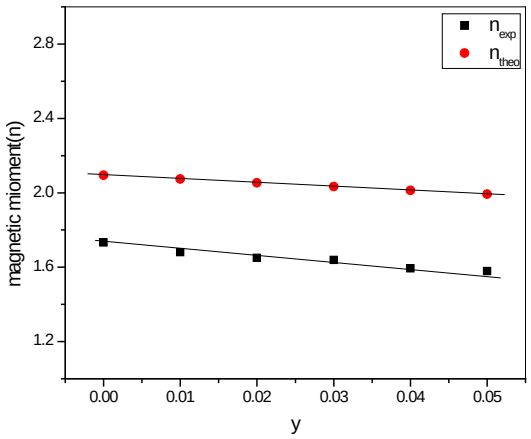

Fig.8. Compositional dependence of the theoretical and experimental magnetic moment at room temperature.

4. Conclusions

1. XRD analysis revealed that the samples have single phase cubic spinel structure for $0.0 \leq y \leq 0.01$ while for $y \geq 0.02$, a small peak of secondary phase ($Gd_3Fe_5O_{12}$) was appeared.
2. The electrical resistivity of the samples (ρ) was increasing gradually with the increasing of Gd content (y) from8.8 $x10^3$ Ω.m to 19.2$x10^3$ Ω.m that reduces the occurrence of the eddy currents and consequently reduces the energy loss as a heat so they can be used in many applications such as transformer cores and memory cores.
3. All the prepared samples show n-type conduction due to the hopping of electron
4. The initial permeability and the magnetic moment of the prepared samples were found to be increases with increasing Gd content up to y= 0.01 and then decreases.
5. The substitution by Gd^{3+} improves the physical properties of the prepared samples where the sample of y= 0.01 exhibits high resistivity, highest initial permeability

References

1. A. Costa, E. Tortella, M.R. Morelli and R. Kiminami: J. Magn. Magn. Mater, **256(3),** 174, (2003).
2. Z. Wang, D. Schiferl, Y.Zhao and H. O'Neill: J. Phys. Chem. of Solids, **64, (12),** 2517,2003.
3. K .Vijaya Kumar and D. Ravinder: Materials Letters, **52,** 166, 2002.
4. D.C. Khan, M. Misra and A. R. Das: J. Appl. Physics, 1982, **53**, 2722, 2002.
5. M. A. Ahmed, K. E. Rady and M. S. Shams: J. Alloy Compd., **622**,269, 2015.
6. A. A. Sattar , H. M. El-Sayed, K.M. El-Shokrofy and M. M. El-Tabey: Journal of materials science, **42(1)**, 149,2007.
7. N. Rezlescu, E. Rezlescu, C. Pasnicu and M. L. Craus: J. Phys.: Condens.Matter, **6**, 5707, 1994.
8. E. Rezlescu, N. Rezlescu, C. Pasnicu, M. L. Craus and P. D. Popa: Crystal Res. Technol., 1996, **31(3)**,343, 1994.
9. S. E. Jacobo, S. Duhalde, S. Duhalde and H. R. Bertorello: J. Magn. Magn. Mater, **276**, 2253, 2004.
10. M .Asif Iqbal, Misbah-ul Islam, Muhammad Naeem Ashiq, Irshad Ali, Aisha Iftikhar and M. Hasan Khan: J. Alloy Compd., **579**, 18, 2013.
11. Z.G. Zheng, X.C. Zhong, Y.H. Zhang, H.Y. Yu and D.C. Zeng, J. Alloy Compd., 466, 377, 2008.
12. O. M. Hemeda, M. Z. Said and M. M. Barakat: J. Magn. Magn. Mater., **224**,132, 2001.
13. L. John Berchmans, R. Kalai Selvan, P. N. Selva Kumar and C. O. Augustin: Materials Letters, **58**, 1928, 2004.
14. R. Islam, M. A. Hakim, M. O. Rahman, Narayan H . Das and M. A. Mamun: J. Alloy Compd., **559**, 174, 2013.
15. N. Rezlescu, E. Rezlescu, C. Pasnicu and M. L. Craus: J. Magn. Magn. Mater., **136**, 319, 2009.
16. M.T. Rahman and C.V. Ramana: Ceramics international, **40(9)**, 14533, 2014.
17. P.P. Hankare, V. T. Vader, U.B. Sankpal, L.V. Gavali, R. Sasikala, I.S. Mulla, Solid state SCi. **11**,2075, 2009.
18. G. C. Jain, B. K. Das, R. S. Khanduja, and S. C. Gupta: J. Mater. Sci., **11,** 1335, 1976.
19. Z. K. Heiba, Mohamed Bakr Mohamed, M. A. Ahmed, M. A. Moussa and H. H. Hamdeh: J. Alloy Compd., **586**,773, 2014.
20. Jagdish Chand, Gagan Kumar, Pawan Kumar, S. K. Sharma, M. Knobel and M. Singh: J. Alloys Comp., **509,** 9638, 2011.
21. S. R. Kulkarni, C. M. Kanamedi, K. K. Patankar and B. K. Chougule: J. Mater. Sci., **40(21)**, 5691, 2011.
22. W. J. Nellis and S. L. Egvold: Phys. Rev., **180**,581, 1969.
23. J. Peng, M. Hojamber Diev., Y. Xu and B. Cao: J. Mag. Mag. Mater., **323**,133, 2001.